Proceedings of the ASME 2011 Dynamic Systems and Control Conference
DSCC2011
October 31 - November 2, 2011, Arlington, VA, USA

DSCC2011-6135

TWO DIMENSIONAL MODELING AND SIMULATION OF A TETHERED AIRFOIL SYSTEM FOR HARNESSING WIND ENERGY

Tuhin K. Das *
Department of Mechanical Engineering
Rochester Institute of Technology
Rochester, NY 14623
Email: tkdeme@rit.edu

Ranjan Mukherjee
Department of Mechanical Engineering
Michigan State University
East Lansing, MI 48824
Email: mukherji@egr.msu.edu

Rahulram Sridhar
Department of Mechanical Engineering
Rochester Institute of Technology
Rochester, NY 14623

Aren Hellum
Department of Mechanical Engineering
Michigan State University
East Lansing, MI 48824

ABSTRACT

A novel wind machine is described in which an airfoil-like kite is tethered to a moving base; the non-conservative nature of the wind loads over a cycle of the kite allows energy to be extracted at the base. A dynamic model for the kite-tether system is derived which models the tether as a series of point masses connected by massless rods. The lift and drag characteristics of the kite are determined from airfoil calculations. The system has been found to be stable via simulation at several wind speeds of interest. A sample base motion which extracts energy from the oncoming wind is also presented.

NOMENCLATURE

m_k	Mass of the airfoil
l_t, m_t	Length and mass of tether
l_e, m_e	Length and mass of each tether element
ϕ_k	Inclination of airfoil with horizontal
ϕ_i	Inclination of i^{th} tether element with horizontal
y_n, z_n	y and z co-ordinates of position of nth tether element
$U_{\infty,y}$	Free stream air velocity component in y direction
$U_{\infty,z}$	Free stream air velocity component in z direction
$U_{rel,y}$	Relative velocity of wind in y direction
$U_{rel,z}$	Relative velocity of wind in z direction
U_{rel}	Free stream air velocity relative to airfoil
L, D	Lift and drag forces acting on the airfoil perpendicular and parallel to the direction of the velocity of the wind relative to the kite
ρ	Free stream air density
C_L, C_D	Co-efficients of lift and drag
A	Airfoil area
α	Angle of attack
$\alpha_{L,0}$	Angle of attack for zero lift
e	Span effectiveness factor
AR	Aspect Ratio
b, s	Wing span and wing area respectively
C_d	Profile drag
T, V	Kinetic and potential energy of the tether-airfoil system
$\mathcal{L}$	Lagrangian
W	Virtual work done by external non-potential forces and torques
τ_i	Generalized force corresponding to generalized coordinate ϕ_i
τ_k	Generalized force corresponding to generalized coordinate ϕ_k
y_c, z_c	Co-ordinates of center of mass of airfoil
y_0	Position of base
F_b	Generalized force corresponding to generalized coordinate y_0
I	Airfoil moment of inertia
M_a	Torque due to offset of L and D from mass center

*Address all correspondence to this author.

Copyright © 2011 by ASME

F_a	Actuation force for changing airfoil inclination
d	Distance of actuation force from airfoil center

INTRODUCTION

Prior to the advent of electrical power, machines were designed to convert the kinetic energy of the wind into useful work. While today's wind turbines are more likely to be connected to a power utility grid than a grindstone, the realizations of wind machines tend to share a familiar design, that of a rotating shaft with some number of blades affixed to a rigid mast-like support. The system described in the present work is a departure from that design, consisting instead of an airfoil-shaped kite tethered to a moving base on the ground. The base and angle of attack of the airfoil are actuated such that for a given path of the kite, net work is done on the base, and the excess work can be extracted.

This use of a tethered element subject to non-conservative forces over a cycle is similar in concept to Ockels' "Laddermill" design [1], which employs a continuous loop of kites. The difference is that the Laddermill employs a fixed base instead of the more general moving base proposed here. A design that uses a single kite tethered to a movable base is found in [2]. The concept is quite similar to the one proposed in this paper. However unlike [2] where the kite is passive entity, we introduce an extra degree of actuation, the actuation of the kite's inclination. Tethered designs have some advantages over standard propeller based designs that warrant their investigation – chief among these is the ability to change the effective deployment altitude, and to exceed the range of feasible heights which can be obtained with a tower. Furthermore, while the design of standard wind turbines is relatively mature, conventional designs have run up against some hard limits, such as the material strength of the blades, which limits the available swept area. The need for large swept area makes transport and manufacture of turbine components difficult, limiting the use of wind power in developing areas. In contrast, the components of tethered kite-like designs are generally flexible, and permit easier transport. The price tethered systems have to pay for these advantages is the need to control the states associated with the tether-airfoil system, both to optimize energy extraction and guarantee that the system does not fall to earth.

A theoretical maximum for the efficiency of a propeller-like turbine was derived by Betz in 1920 [3], whose analysis predicted that at most 59.3% of the energy of the oncoming wind could be converted by such a device into usable energy. Betz' analysis is based on an idealized actuator disk, which assumes that the oncoming wind is diffused across the disk and that the difference in kinetic energy across the disk is extracted as usable work. Loyd [4] analyzed an apparatus similar to that proposed here, and points out that the assumptions used in Betz' analysis are not germane to a kite-like wind machine. He proposes an alternate definition of efficiency for such a machine, equal to the fraction of the kite's load which is delivered to the shaft. Loyd found that a kite of similar size to a large aircraft could produce more than 3 MW of power in a 10 m/s wind, a similar figure to that produced by large propeller-like devices. Both Loyd's work and that of a more recent paper by Argatov et al. [5] assume that the tether is straight at all times. Argatov's work solves for the power produced by a "pumping" kite generator, and analytically finds expressions for the power produced by such a system, assuming a known kite trajectory and angle of attack.

A small-scale test of a tethered kite system was described by Canale et al. [6], who used a fully flexible kite similar to the ram airfoil kites used by kiteboarders. The kite was employed in what they call the "yo-yo" configuration, in which a stationary base controls the attitude of the kite and line tension in such a way that energy is extracted. They found that they were able to extract energy, note that a scaled-up version of their test system could produce 2 MW of power with a 500 m^2 kite. That paper also provides analysis for the "carousel" configuration, in which multiple kites are allowed affixed to a common base which is free to rotate, and power is extracted from the rotation of that base, effectively forming a large vertical-axis turbine.

In this paper, we discuss a simple dynamic model of a two-dimensional tether-airfoil system mounted on a base capable of linear horizontal motion. The aerodynamic lift and drag forces on the airfoil are also discussed in detail. Through a simulation based study the existence of stable equilibrium configurations is verified. Subsequently, we demonstrate through simulations that net energy can be extracted by synchronous periodic actuation of the base and the inclination angle of the airfoil. This paper is organized as follows. We first provide details of the dynamic model of the tether-airfoil system. Next we develop the formulations of lift and drag forces and corresponding lift and drag coefficients. Thereafter, simulation results are given. Through simulations we first verify the existence of equilibrium configurations and their stability in the presence of perturbations. Next we show the feasibility of net energy extraction through base actuation. Lastly, we provide concluding remarks.

TETHER AIRFOIL SYSTEM MODELING

Assumptions

We assume a tether-airfoil system as shown in Fig.1. For modeling the system and investigating the possibility of energy extraction, we make the following assumptions:

A1. The tether-airfoil system moves entirely within the yz-plane.
A2. The airfoil is a square, flat plate, and its instantaneous angle with respect to the oncoming wind is sufficiently small that the the foil is not in a stalled condition.
A3. The tether is assumed to be inextensible and composed of point masses connected by massless rods. The tether is negligibly thin and is not subject to aerodynamic loads.
A4. The response times of the controllers used to move the base and pitch angle of the airfoil are much less than the time scales characteristic of the dynamic system and are ignored.
A5. The velocity of the oncoming wind has time-steady magnitude and direction.

Copyright © 2011 by ASME

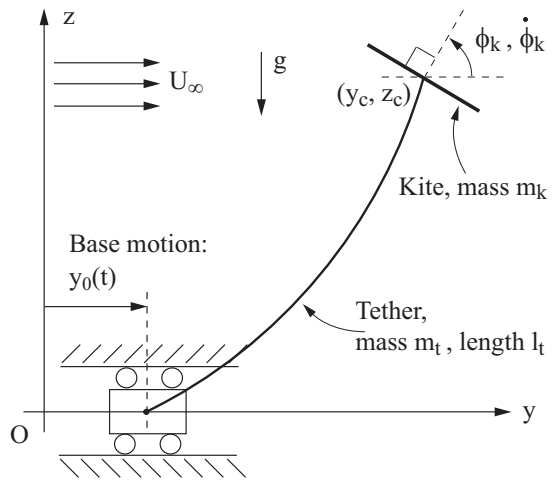

Figure 1. SCHEMATIC OF TETHER-AIRFOIL SYSTEM

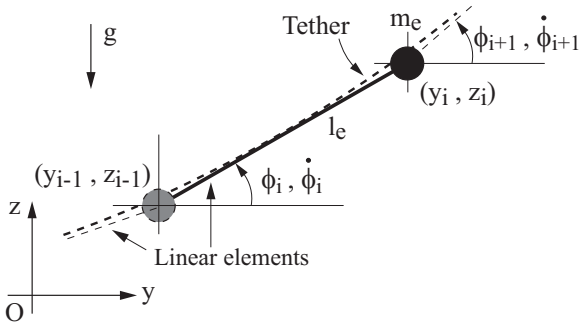

Figure 2. SPATIAL ORIENTATION OF A SINGLE TETHER ELEMENT

A6. The kite has a control-system (sensors and actuators) that allows it to control the inclination of the kite with the horizontal.

Dynamic model - Lagrangian Formulation

In this section, a mathematical model of the tether-airfoil system, shown in Fig. 1, is derived. A discretized tether with $n+1$ tether elements is modeled. A single tether element is shown in Fig. 2. Each element of the tether has a length $l_e = l_t/(n+1)$. The first n point masses having mass $m_e = m_t/(n+1)$ and the $(n+1)^{\text{th}}$ point mass has a mass of $m_{n+1} = m_e + m_k$. Consider a single, discrete tether element as shown in Fig. 2. The position of the i^{th} point mass relative to the absolute co-ordinate axes can be written as

$$y_i = l_e \sum_{j=1}^{i} \cos\phi_j + y_0, \quad z_i = l_e \sum_{j=1}^{i} \sin\phi_j \qquad i = 1,2,\ldots,(n+1) \tag{1}$$

from which the velocity equations follow directly as

$$\dot{y}_i = -l_e \sum_{j=1}^{i} \dot{\phi}_j \sin\phi_j + \dot{y}_0, \quad \dot{z}_i = l_e \sum_{j=1}^{i} \dot{\phi}_j \cos\phi_j \qquad i = 1,2,\ldots,(n+1) \tag{2}$$

Define $\phi_i,\ i = 1,2,\ldots,(n+1)$, y_0 and ϕ_k as the generalized co-ordinates for deriving the equations of motion. Also define the Lagrangian $\mathcal{L} = T - V$. Then, the Lagrange's equation for the generalized co-ordinate ϕ_i is written as

$$\frac{d}{dt}\left(\frac{\partial \mathcal{L}}{\partial \dot{\phi}_i}\right) - \frac{\partial \mathcal{L}}{\partial \phi_i} = \tau_i, \quad i = 1,2,\ldots,(n+1) \tag{3}$$

while that for the generalized co-ordinates y_0 and ϕ_k are

$$\frac{d}{dt}\left(\frac{\partial \mathcal{L}}{\partial \dot{y}_0}\right) - \frac{\partial \mathcal{L}}{\partial y_0} = F_b, \quad \frac{d}{dt}\left(\frac{\partial \mathcal{L}}{\partial \dot{\phi}_k}\right) - \frac{\partial \mathcal{L}}{\partial \phi_k} = \tau_k \tag{4}$$

The net kinetic energy of the tether-airfoil system is

$$T = \frac{1}{2} m_e \left[\sum_{i=1}^{n} (\dot{y}_i^2 + \dot{z}_i^2)\right] + \frac{1}{2} m_{n+1} (\dot{y}_{n+1}^2 + \dot{z}_{n+1}^2) + \frac{1}{2} I \dot{\phi}_k^2 \tag{5}$$

where $\dot{y}_i$ and $\dot{z}_i$ are defined in Eq. (2). Similarly the net potential energy of the tether-airfoil system is

$$V = m_e g \sum_{i=1}^{n} z_i + m_{n+1}\, g\, z_{n+1} \tag{6}$$

where z_i is defined in Eq. (1). From Eqs. (3), (5) and (6), we have the following equation of motion of the generalized co-ordinates ϕ_i

$$\begin{aligned}
&m_e l_e^2 (n-i+1) \textstyle\sum_{j=1}^{i} \sin(\phi_i - \phi_j) \dot{\phi}_j^2 \\
&+ m_e l_e^2 \textstyle\sum_{j=i+1}^{n} \left[\sin(\phi_i - \phi_j) \dot{\phi}_j^2 (n-j+1)\right] \\
&+ m_e l_e^2 (n-i+1) \textstyle\sum_{j=1}^{i} \cos(\phi_i - \phi_j) \ddot{\phi}_j \\
&+ m_e l_e^2 \textstyle\sum_{j=i+1}^{n} \left[\cos(\phi_i - \phi_j) \ddot{\phi}_j (n-j+1)\right] \\
&+ (m_e + m_k) l_e^2 \textstyle\sum_{j=1}^{n+1} \cos(\phi_i - \phi_j) \ddot{\phi}_j \\
&+ (m_e + m_k) l_e^2 \textstyle\sum_{j=1}^{n+1} \sin(\phi_i - \phi_j) \dot{\phi}_j^2 \\
&+ m_e g l_e (n-i+1) \cos\phi_i + (m_e + m_k) g l_e \cos\phi_i \\
&- l_e \sin\phi_i \ddot{y}_0 \left[m_e (n-i+1) + m_e + m_k\right] = \tau_i \\
&\quad i = 1,2,\ldots,(n+1)
\end{aligned} \tag{7}$$

Additionally, we have from Eq. (4), (5) and (6), the following equations of motion of the generalized co-ordinates y_0 and ϕ_k

$$\begin{aligned}
&m_e \textstyle\sum_{i=1}^{n} \ddot{y}_i + (m_e + m_k)\, \ddot{y}_{n+1} + \left[m_e (n+1) + m_k\right] \ddot{y}_0 = F_b, \\
&I \ddot{\phi}_k = \tau_k
\end{aligned} \tag{8}$$

Copyright © 2011 by ASME

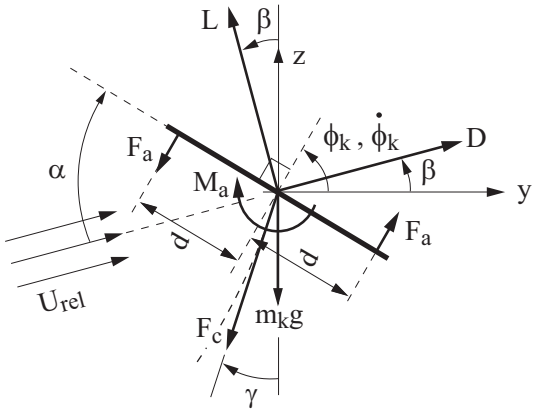

Figure 3. FREE-BODY DIAGRAM OF AIRFOIL

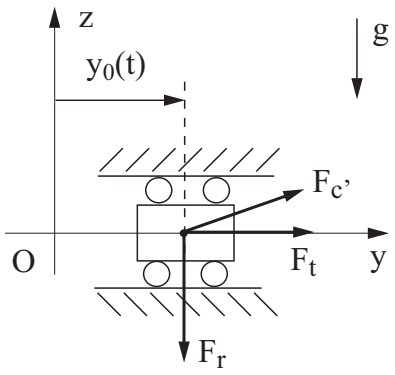

Figure 4. FREE-BODY DIAGRAM OF BASE

Next, in order to determine the generalized torques τ_i, τ_k and the generalized force F_b, we apply the *Principle of Virtual Work* [7]. First, the external non-potential forces and torques are identified from free-body diagrams of the airfoil and the base shown in Figs.3 and 4. The non-potential forces and torques are L, D, F_a, M_a, F_r and F_t. Defining force $\vec{F}$ as

$$\vec{F} = (D\cos\beta - L\sin\beta)\,\hat{j} + (D\sin\beta + L\cos\beta)\,\hat{k} \tag{9}$$

we can write the following expression of virtual work done by non-potential forces and torques

$$\delta W = \vec{F}\cdot\left(\delta y_c\,\hat{j} + \delta z_c\,\hat{k}\right) + F_t\,\delta y_0 + (2F_a d - M_a)\,\delta\phi_k \tag{10}$$

where, from Eq.(1),

$$y_c = l_e\sum_{j=1}^{n+1}\cos\phi_j + y_0, \quad z_c = l_e\sum_{j=1}^{n+1}\sin\phi_j. \tag{11}$$

The virtual displacements δy_c and δz_c are expressed in terms of virtual displacements of generalized coordinates using Eq. (1), as follows

$$\delta y_c = -l_e\sum_{i=1}^{n+1}\sin\phi_i\delta\phi_i + \delta y_0, \quad \delta z_c = l_e\sum_{i=1}^{n+1}\cos\phi_i\delta\phi_i \tag{12}$$

Carrying out the dot product in Eq.(10) and extracting the coefficient of $\delta\phi_i$, we get the following expression for τ_i

$$\tau_i = -l_e[(D\cos\beta - L\sin\beta)\sin\phi_i - (D\sin\beta + L\cos\beta)\cos\phi_i] \tag{13}$$

Similarly, since the generalized force F_b is associated with the generalized coordinate y_0, extracting the coefficient of δy_0 from Eq.(10), we have

$$F_b = D\cos\beta - L\sin\beta + F_t \tag{14}$$

Finally, the generalized torque τ_k of Eq.(8) is obtained by extracting the coefficient of $\delta\phi_k$

$$\tau_k = 2F_a d - M_a \tag{15}$$

It is worth noting here that the cable tension is not included in the calculation of the generalized forces and torques since it is an internal force for the tether airfoil system. Eqs. (7), (8), (13), (14) and (15), the equation of motion of the tether-airfoil model is completely defined.

LIFT AND DRAG FORMULATION

This section is devoted to the modeling of lift (L) and drag (D) forces acting on the airfoil. The directions of D and L are parallel and perpendicular respectively to the direction of relative wind speed U_{rel} with respect to the airfoil, as shown in Figure. 3, [8]. From Eq. (11), U_{rel} is obtained as:

$$\begin{aligned} U_{rel,y} &= (U_{\infty,y} - \dot{y}_c) = U_{\infty,y} + l_e\textstyle\sum_{j=1}^{n+1}\dot{\phi}_j\sin\phi_j - \dot{y}_0 \\ U_{rel,z} &= (U_{\infty,z} - \dot{z}_c) = U_{\infty,z} - l_e\textstyle\sum_{j=1}^{n+1}\dot{\phi}_j\cos\phi_j \\ \vec{U}_{rel} &= U_{rel,y}\,\hat{j} + U_{rel,z}\,\hat{k} \end{aligned} \tag{16}$$

The lift and drag forces acting on the airfoil are, [8]

$$L = \frac{1}{2}\rho C_L A\|\vec{U}_{rel}\|^2, \quad D = \frac{1}{2}\rho C_D A\|\vec{U}_{rel}\|^2 \tag{17}$$

where,

$$\|\vec{U}_{rel}\|^2 = U_{rel,y}^2 + U_{rel,z}^2$$

The calculation of C_L and C_D are discussed next.

Copyright © 2011 by ASME

Calculation of Coefficient of Lift

For an infinite wing, from [8],

$$C_L \approx 2\pi(\alpha - \alpha_{L,0}) \tag{18}$$

where the slope $dC_L/d\alpha = 2\pi$ is obtained from the *Thin Airfoil Theory* discussed in [8] and $\alpha_{L,0}$ is obtained from experimental data. For a finite wing, $\alpha_{L,0}$ remains the same. However, unlike in the case of an infinite wing,

$$\frac{dC_L}{d\alpha} = \frac{2\pi}{1+\frac{2}{eAR}}, \quad AR = \frac{b^2}{s} \tag{19}$$

where e is obtained from experimental data, and with typical values in the range $0.8 \leq e \leq 1$. See [9].

Calculation of Coefficient of Drag

The drag co-efficient of the airfoil comes from two drag components namely the profile drag and the induced drag. The equation for drag co-efficient is, [9]

$$C_D = C_d + \frac{{C_L}^2}{\pi eAR} \tag{20}$$

where the first term, C_d, of Eq. (20) is the profile drag and the second term is the induced drag.

SIMULATION RESULTS

Before presenting the simulation results, the specific formulae for C_L and C_D developed for this model are given. We assume a square shaped wing span with one of the corners facing the head wind. For a square of side a, from Eq. (19) $AR = (\sqrt{2}a)^2/a^2 = 2$. The parameter e is taken as 0.8 and $\alpha_{L,0}$ as -0.035rad ($\approx -2^\circ$) based on experimental data from various NACA airfoils presented in [8,9]. Upon substituting these values into Eq. (19), the following relation is obtained for C_L:

$$C_L = 2.793(\alpha + 0.035) \tag{21}$$

The profile drag C_d was obtained from [10] based on experimental data presented for a selection of NACA airfoils for a Reynolds number of the order of 10^6. This value of Reynolds number was chosen specific to this application by computing the range of Reynolds numbers for expected wind speeds varying from 10m/s to 30m/s. The profile drag is then given by

$$C_d = 0.1943\alpha^2 + 0.00625 \tag{22}$$

Table 1. FIXED PARAMETER VALUES

Parameter	Value
l_t	100 m
m_t	0.5 kg
I	2.5 kgm^2
d	0.5 m
ρ	1.3 kgm^{-3}
$n+1$	10

From Eqs.(20), (21) and (22), C_D can be expressed as

$$C_D = 0.1943\alpha^2 + 0.00625 + 0.199{C_L}^2 \tag{23}$$

Substituting for C_L and C_D from Eqs.(21) and (23) into Eq.(17), the required lift and drag forces on the airfoil are obtained.

Table 1 shows the fixed parameter values for the tether-airfoil system employed. We next investigate the stability of equilibrium configurations of the system by simulating the effects of perturbations. This is followed by simulations to demonstrate the feasibility of energy extraction through base actuation.

Investigation of Stability - Effect of Perturbations

In this section, simulation is carried out for a wind speed of $U_{\infty,y} = 10$ m/s and $U_{\infty,z} = 0$ m/s with a step increase to $U_{\infty,y} = 11$ m/s at $t = 200$ s. The parameter values specific to this simulation are $m_k = 5$ kg, and $A = 1.5$ m^2. Also, since there is no base actuation, we have $y_0(t) = 0$. The initial conditions for this simulation are $\phi_i(0) = 0.5$ rad, and $\dot{\phi}_i(0) = 0$ rad/s for $i = 1, 2, \cdots, 10$. Also, airfoil inclination is constant at $\phi_k = 80^\circ$. Figure 5 shows the resulting plots. As expected, with the step increase in wind speed, Fig.5(a) suggests that the tether becomes more taut as the range of ϕ_i, $i = 1, 2, \cdots, 10$, decreases with the step increase. Note in Fig.5(c) that F_t remains negative. From Fig.4, this confirms that tether is always in tension. The effective angle of attack α is plotted in Fig.5(d), showing its variation during transients before its settles to the equilibrium value of $90^\circ - \phi_k = 12^\circ$. The coordinates of the center of mass of the kite (y_c, z_c) are plotted against each other and against time in Figs.5(e) and 5(f) respectively. The simulation results show the convergence of the tether-airfoil system to stable equilibrium configurations under perturbations introduced through initial conditions or as change in wind speed.

We next derive the individual equilibrium values for ϕ_i and (y_c, z_c). For equilibrium, we have $\dot{\phi}_k = 0$, $\ddot{\phi}_k = 0$ and $\beta = 0$ in Eqs. (7) and (13). Thus, at equilibrium

$$m_e g l_e (n-i+1)\cos\phi_i + (m_e + m_k) g l_e \cos\phi_i = \tau_i \tag{24}$$

Copyright © 2011 by ASME

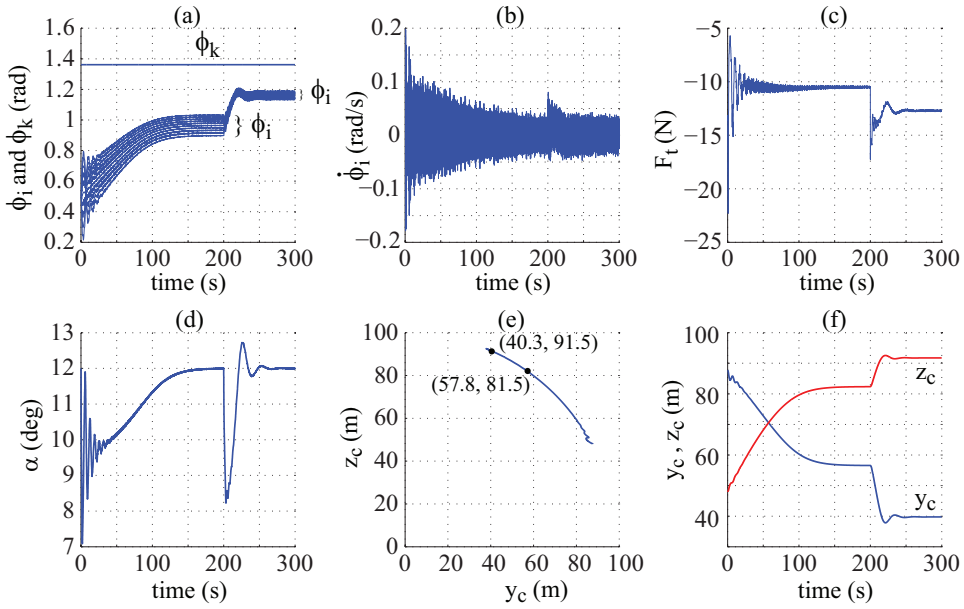

Figure 5. TETHER-AIRFOIL SYSTEM SIMULATION UNDER PERTURATIONS

Solving for ϕ_i, we have the following equilibrium points

$$\phi_i = \arctan\left[\frac{L-(m_e g\,(n-i+2)+m_k g)}{D}\right] \tag{25}$$

$\forall\, i = 1,2,\ldots,10$. Upon substituting for the parameter values we obtain the equilibrium ϕ values as well as the equilibrium position of the center of mass of the airfoil (y_c, z_c). The plot of the equilibrium ϕ_i values for the different tether elements for $U_{rel} = 10$ m/s and $U_{rel} = 11$ m/s is shown in Fig.6 The equilibrium position of the center of mass of the airfoil is obtained as $(57.8, 81.48)$m when $U_{\infty,y} = 10$ m/s and $(40.32, 91.49)$m when $U_{\infty,y} = 11$ m/s, and are indicated also on Fig.5(e).

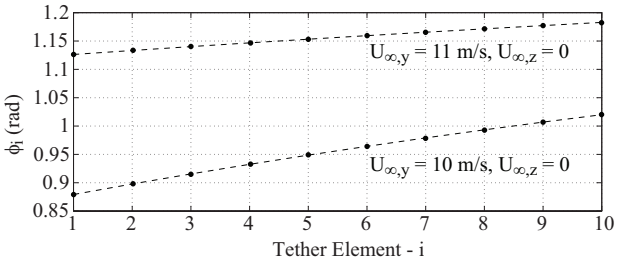

Figure 6. EQUILIBRIUM ϕ VALUES FOR DIFFERENT TETHER ELEMENTS FOR TWO DIFFERENT WIND SPEEDS

Energy Extraction through Base Actuation

Next we demonstrate the feasibility of energy extraction from the tether-airfoil system using base actuation and simultaneous synchronized actuation of ϕ_k. For this simulation, we assume the parameter values of Table 1 and the parameter values specific to this simulation are $m_k = 3$kg, and $A = 25$m^2. These values are chosen different from those used for the stability investigation presented earlier just to show that considerable energy extraction is possible. We assume $U_{\infty,y} = 17$ m/s and $U_{\infty,z} = 0$ m/s. The initial conditions for this simulation are $\phi_i(0) = 1.3$rad, and $\dot{\phi}_i(0) = 0$rad/s for $i = 1,2,\cdots,10$. In the simulation, we allow the system to converge to equilibrium and subsequently at $t = 150$s we initiate a sinusoidal base actuation of amplitude 6 m and frequency 0.2Hz. Thus,

$$y_0(t) = \begin{cases} 0 & \text{for } t < 150 \text{ s} \\ 6\sin\left(0.4\pi(t-150)\right) & \text{for } t \geq 150 \text{ s} \end{cases} \tag{26}$$

Simultaneously, the angle of inclination ϕ_k is varied in synchronization with the base motion, with an amplitude of 6.5° but with a phase shift of 110°, as follows

$$\phi_k = \begin{cases} 75^\circ & \text{for } t < 150 \text{ s} \\ 81.11^\circ - 6.5^\circ \sin\left(0.4\pi(t-150)+110^\circ\right) & \text{for } t \geq 150 \text{ s} \end{cases} \tag{27}$$

The amplitude and phase shift of ϕ_k actuation were chosen to provide significant energy extraction but were not optimized. From Eqs.(8) and (15), the above designed trajectory of ϕ_k can be ideally achieved by designing the actuation force F_a as

$$F_a = \frac{I\ddot{\phi}_k + M_a}{2d} \tag{28}$$

Copyright © 2011 by ASME

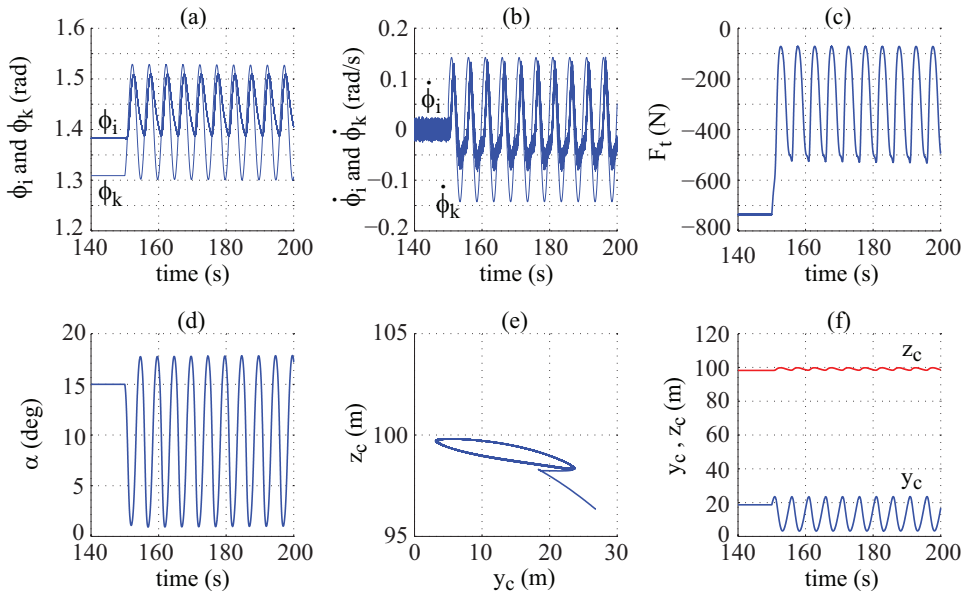

Figure 7. TETHER-AIRFOIL SYSTEM SIMULATION UNDER BASE ACTUATION

This idealized F_a is used in this work. However, in practice, a feedback controller must be used to track a desired ϕ_k trajectory such as the one in Eq.(27). The response of the system is shown in Fig.7. The individual plots are self-explanatory. As expected, due to the higher wind speed of 17m/s used in this simulation compared to Fig.5, the tether is more taut and hence ϕ_i, where $i = 1, 2, \cdots, 10$, are almost equal to each other. The high wind speed provides greater lift force and hence the airfoil hovers at a higher altitude, Fig.7(e) and 7(f) as compared to Fig.5. It also leads to a larger magnitude of F_t as shown in Fig.7(c). The energy extracted is obtained from the integral

$$E_{ex} = \int_0^t F_t \dot{y}_0 dt \tag{29}$$

and is plotted in Fig.8. A negative value of the integral indicates a net energy extraction. Also, the slope of E_{ex} gives an indication of the power generated. As seen in Fig.8, the power generated is approximately 800W for the simulation shown. It is noted that the energy extraction can be maximized through selection of optimum design parameters or through control/actuation optimization. However, the focus of this paper is only to show the feasibility of energy extraction and such optimization studies as mentioned above are topics of future research.

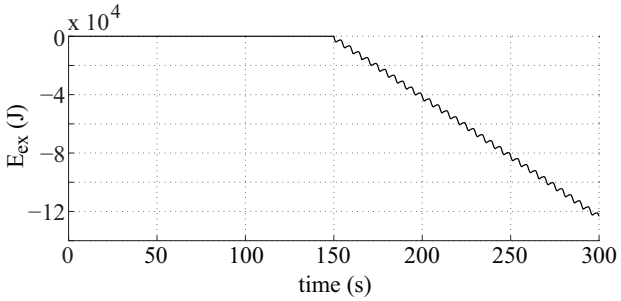

Figure 8. WIND ENERGY EXTRACTED THROUGH BASE ACTUATION

CONCLUSION

A non-conservative tethered wind machine has been described and shown to be stable for several wind speeds in the range of interest. An open-loop trajectory for the moving base is presented which extracts energy from the flow. We plan to extend many of the preliminary results found in this work, such as a general proof of the system's stability rather than the empirical method used here. This has already been undertaken for a simple straight cable, and we are currently working on an extension to a flexible cable. A closed-loop controller for the system's base must be developed and optimized, and all derivations must eventually be extended to three dimensions.

It bears mention that the advantages of this type of machine over conventional turbines is in siting rather than efficiency; evaluated on a power per area metric, the trajectory we describe in the paper extracts less energy than a standard turbine of equal size. However, the deployment flexibility of these systems allows them to extract energy at greater heights than standard turbines, an advantage in developed areas, where neighboring buildings both reduce the kinetic energy of the wind and make its direction unpredictable. We therefore believe in the promise of this class of devices and that the simplified system presented here represents an interesting addition to the body of papers on non-conservative wind machines.

Copyright © 2011 by ASME

REFERENCES

[1] Ockels, W., 2001. "Laddermill, a novel concept to exploit the energy in the airspace". *Aircraft Design,* **4**, pp. 81–97.

[2] Willams, P., Lansdorp, B., and Ockels, W., 2008. "Optimal cross-wind towing and power generation with tethered kites". *AIAA Journal of Guidance, Control and Dynamics,* **31**(1).

[3] Betz, A., 1920. "Das maximum der theoretisch mo'glichen ausnutzung des windes durch windmotoren". *Zeitschrift fur das gesamte Turbinenwesen,* **26**.

[4] Loyd, M., 1980. "Crosswind kite power". *Journal of Energy,* **4 (3)**, pp. 106–111.

[5] Argatov, I., Rautakorpi, P., and Silvennoinen, R., 2009. "Estimation of the mechanical energy output of the kite wind generator". *Renewable Energy,* **34 (6)**, pp. 1525–1532.

[6] Canale, M., Fagiano, L., and Milanese, M., 2010. "High altitude wind energy generation using controlled power kites". *IEEE Transactions on Control Systems Technology,* **18 (2)**, pp. 279–293.

[7] Meirovitch, L., 1970. *Methods of Analytical Dynamics*. McGraw-Hill, New York.

[8] Anderson Jr., J. D., 2010. *Fundamentals of Aerodynamics*, 5th ed. McGraw-Hill.

[9] Anderson Jr., J. D., 2011. *Introduction to Flight*, 7th ed. McGraw-Hill.

[10] White, F., 2002. *Fluid Mechanics*, 5th ed. ed. McGraw-Hill.

Copyright © 2011 by ASME